

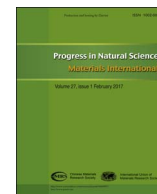
HOSTED BY



ELSEVIER

Contents lists available at ScienceDirect

## Progress in Natural Science: Materials International

journal homepage: [www.elsevier.com/locate/pnsmi](http://www.elsevier.com/locate/pnsmi)

## Original Research

Influence of withdrawal rate on the porosity in a third-generation Ni-based single crystal superalloy<sup>☆</sup>Quanzhao Yue<sup>a</sup>, Lin Liu<sup>a,\*</sup>, Wenchao Yang<sup>a,\*</sup>, Taiwen Huang<sup>a</sup>, Jun Zhang<sup>a</sup>, Hengzhi Fu<sup>a</sup>, Xinbao Zhao<sup>b</sup><sup>a</sup> State Key Laboratory of Solidification Processing, Northwestern Polytechnical University, Xi'an 710072, Shaanxi Province, China<sup>b</sup> Xi'an Thermal Power Research Institute Co. Ltd., Xi'an 710032, Shaanxi Province, China

## ARTICLE INFO

## Keywords:

Superalloys  
Porosity  
Withdrawal rate  
Microstructure  
Quantitative evaluation

## ABSTRACT

The influence of withdrawal rate on the porosity in a third-generation Ni-based single crystal superalloy was investigated by a quantitative evaluation method. The results showed that the withdrawal rate obviously effected on the average area fraction, number and diameter of porosities except their radius ratios. In consideration of the microstructure observation for dendrite arms, an optimized withdrawal rate was obtained with a minimum porosity level as about  $125 \mu\text{m s}^{-1}$ . Simultaneously, a threshold value for the acceptance level of porosities might be set as about 0.1% in order to fulfill the requirements for Ni-based single crystal casting in laboratory scale. Finally, the formation reason of porosity was discussed and it was concluded that the feeding for the volume shrinkage of the last solidified eutectic liquids from the residual liquids and the isolating effect of the morphologies of dendrite arms might be two key factors in controlling the porosities level in Ni-based single crystal superalloy.

## 1. Introduction

Ni-based single crystal blades are widely used to the hot stage of stationary gas turbines and gas turbine aeroengines for their good mechanical properties, high temperature capability and high environment degradation resistance [1,2]. Nowadays, the single crystal blades are mainly fabricated using the directional solidification technology in the Bridgman furnace. During the process of solidification, the porosities could form inevitably, which are difficult to be compensated by the interdendritic liquid flow [3]. Undoubtedly, these porosities deteriorate seriously the thermal-mechanical properties of turbine blades, especially for the fatigue property [4–6]. It is well known that the formation of porosity mainly depends on the thermal gradient, withdrawal rate and shrinkage factor of the alloy. Based on the investigations for the columnar grain blades fabricated in CMSX-6, Roskosz [7] suggested that the volume fraction of porosity could not exceed 0.145%, which was a sufficient value to fulfill the acceptance requirements for blades. In terms of Ni-based single crystal superalloy, the porosity is different from that in columnar superalloys due to the absence of grain boundaries. Although the average volume fraction values of porosity under certain casting conditions have been found in CMSX-10 (0.3%) and MC-NG single crystal superalloy (0.28%) [8,9],

there is still a lack of a threshold value for Ni-based single crystal superalloys in order to fulfill the acceptance requirements.

Currently, many efforts have been performed to research the porosity in directionally solidified and single crystal Ni-based superalloys. Based on the pressure drop evaluation of the interdendritic liquids, Lecomte-Beckers [10] proposed a porosity index  $\Delta P^*$ , suggesting that the influences of the solidification range and the tortuosity were actually of the most importance factors, where the “tortuosity” is an estimation of the soundness of the feeding channels for the volume shrinkage of the last solidified liquid [11]. Accordingly, with the increase of withdrawal rate and tortuosity, the level of porosity should present a substantial increase. However, Ho [12] believed that the porosity was strongly influenced by the temperature gradient rather than the other factors. On the contrary, Whitesell [13] considered that the pressure drop resulting from the capillary flow could not exhibit a meaningful effect on porosity formation. And, the segregation of dissolved gases and precipitation of gas bubbles played a dominant role in the formation of porosity. However, the interval of the withdrawal rates was too large to obtain abundant dendrite microstructures for investigating the formation of porosity. Further, Anton [3] believed that the low solution of gas in Ni-based superalloys and the vacuum melting could minimize the formation of porosities. As a consequence,

<sup>☆</sup> Peer review under responsibility of Chinese Materials Research Society.

\* Corresponding author.

E-mail addresses: [linliu@nwpu.edu.cn](mailto:linliu@nwpu.edu.cn) (L. Liu), [wenchaoyang@nwpu.edu.cn](mailto:wenchaoyang@nwpu.edu.cn) (W. Yang).<http://dx.doi.org/10.1016/j.pns.2017.02.008>

Received 7 September 2016; Received in revised form 17 February 2017; Accepted 28 February 2017

1002-0071/ © 2017 Published by Elsevier B.V. on behalf of Chinese Materials Research Society This is an open access article under the CC BY-NC-ND license (<http://creativecommons.org/licenses/by-nc-nd/4.0/>).

there were many factors to influence the level of porosity. Among these factors, the effect of withdrawal rate on porosity, which is a very effective method in control the microstructures of the specimen [14], is of great significance in engineering, especially for the large industrial castings [9]. Therefore, some work still needs to be performed to research the effect of withdrawal rate on the porosity.

Actually, Bachalet [15] proposed that there might be an optimum withdrawal rate for a certain alloy and casting, which resulted in the closely spaced dendrite arms and a minimum level of porosity. For example, an optimum withdrawal rate of  $50\text{--}100\text{ }\mu\text{m s}^{-1}$  was found in directional solidified columnar castings of Mar-247 alloy [16]. However, the solidification characteristics have been changed for the third-generation Ni-based single crystal superalloys because of more refractory elements addition [17]. Although there were many investigations concerning the effect of withdrawal rate on the dendrite microstructures [14,18,19], there were few studies to focus the influence of withdrawal rate on the porosity and the interaction between porosities and the dendrite microstructures, especially, for the third-generation Ni-based single crystal superalloys.

Therefore, the aim of this paper was to investigate systematically the size, shape and distribution of porosities in a third-generation Ni-based single crystal superalloy fabricated at different withdrawal rates. The effects of withdrawal rate on the dendrite microstructure, the porosity and the interaction between them were researched and then the formation mechanism of the shrinkage porosity was also discussed.

## 2. Experimental

The chemical compositions of the Ni-based single crystal superalloy named as “Alloy A” used in this investigation were presented in Table 1. Rectangular plate samples with 30 mm in length, 10 mm in width, and 100 mm in height were prepared by the directional solidification technology in the [001] direction with a spiral tail in a high rate directional solidification (HRS) furnace. Withdrawal rates were set as  $50\text{--}150\text{ }\mu\text{m s}^{-1}$  at intervals  $25\text{ }\mu\text{m s}^{-1}$  and  $200\text{ }\mu\text{m s}^{-1}$ . The thermal gradient was estimated about  $40\text{--}50\text{ K cm}^{-1}$  at the front of the solid-liquid interface [20].

The transversal and longitudinal sections were cut by spark erosion in the middle of the castings. Standard metallographic techniques were employed for the preparation of the samples, being capable of removing completely the surface hardening zone. The samples were etched using  $\text{HNO}_3$ : HF: glycerol (1:2:3 in volume). Finally, the metallographic microstructures were observed by optical microscopy (OM) and scanning electron microscopy (SEM). The total specimen surface on polished state was scanned (about  $300\text{ mm}^2$ ) using Olympus LEXT OLS 4000. Then, the images were split into  $4\times 10$  parts as described in Reference [21]. Fig. 1 presented a micrograph of porosities of Alloy A when the withdrawal rate was set as  $125\text{ }\mu\text{m s}^{-1}$ . Excellent contrast could be observed between the porosities and the polished surface, yielding highly reliable results as displayed in Fig. 1. Quantitative evaluation was conducted using Image Pro Plus 6.0 software, and porosities below  $5.2\text{ }\mu\text{m}$  diameter were rejected. And, the dendrite spacings were calculated by the triangle method described in Reference [22].

**Table 1**

The chemical compositions of the single crystal Ni-based superalloys Alloy A (wt%).

	Cr	Co	Mo	W	Ta	Re	Hf	Al	Ti	Ni
Alloy A (wt%)	3.0	12.0	1.0	6.0	8.0	4.0	0.1	6.0	–	Bal.

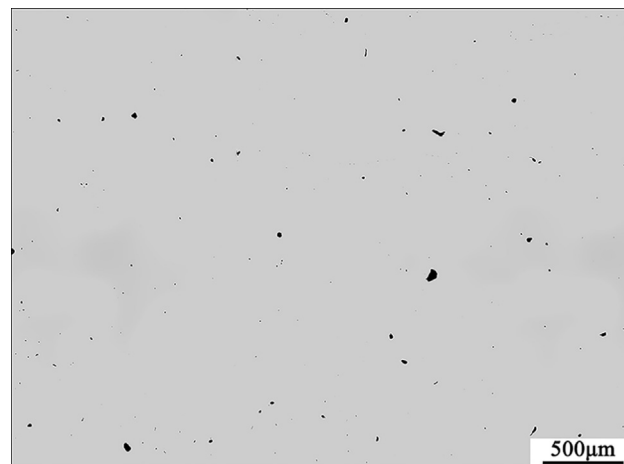


**Fig. 1.** Optical micrograph of porosities of Alloy A fabricated at  $V_s = 125\text{ }\mu\text{m s}^{-1}$  captured by Olympus OLS 4000.

## 3. Results and discussion

### 3.1. As-cast microstructures

The as-cast microstructures of single crystal rectangle plate castings prepared at different withdrawal rates from  $50$  to  $200\text{ }\mu\text{m s}^{-1}$  were shown in Fig. 2. It was clear that the dendrite arms were in alignment when the withdrawal rate was less than  $100\text{ }\mu\text{m s}^{-1}$  at transverse sections. The magnitude of the primary dendrite arm spacings (PDAS) in width direction (about  $415\text{ }\mu\text{m}$ ) was larger slightly than that in length direction (about  $380\text{ }\mu\text{m}$ ) at  $50\text{ }\mu\text{m s}^{-1}$ , as shown in Fig. 2(a<sub>1</sub>). Because the width (10 mm) of the cross section of the rectangle plate casting was smaller than its length (30 mm), it made the heat extraction much easier in width direction. With the increase of withdrawal rate from  $50\text{ }\mu\text{m s}^{-1}$  to  $100\text{ }\mu\text{m s}^{-1}$ , the dendrite arms presented generally a refiner arrangement, as shown in Fig. 2(a<sub>1</sub>–c<sub>1</sub>). Further, when the withdrawal rates were set as 125 and  $150\text{ }\mu\text{m s}^{-1}$ , the dendrite arms were closely spaced and ordered, which presented obviously a hexagonal arrangement where the secondary dendrite arms were nested as shown in Fig. 2(d<sub>1</sub>, e<sub>1</sub>). Moreover, it was found that there were some adequate grown tertiary dendrite arms, which was consistent with the report in reference [21]. When the withdrawal rates were set as  $200\text{ }\mu\text{m s}^{-1}$ , it was observed that the tertiary dendrite arms were strongly developed away from the centerline of the casting, as shown in edge zones below the white short-dash in Fig. 2(f<sub>1</sub>), which resulted from the curved solid/liquid interface at a higher withdrawal rate [2,22]. The concave solid/liquid interface in shape along the withdrawal direction would have the secondary even tertiary dendrite arms growing preferentially toward the center [23], as marked black arrow in Fig. 2(f<sub>1</sub>). As a consequence, it was difficult to measure precisely the PDAS and secondary dendrite arm spacings (SDAS) at withdrawal rate  $200\text{ }\mu\text{m s}^{-1}$ . And the dendrite arms were loosely arranged in some interdendritic areas (denoted as defective areas), as indicated by the white circles in Fig. 2(e<sub>1</sub>, e<sub>2</sub>, f<sub>1</sub>, f<sub>2</sub>), which provided more space for the emergence and continued growth of porosities. It's clearly that there are more defective areas in specimen with concave solid/liquid interface, as shown in Fig. 2(f<sub>1</sub>), which might be due to the poor soundness of the feeding channels resulting from the dendrite coherency [24] of the inward over-growth of the secondary dendrite arms in edge zones. In addition, the corresponding microstructures with different withdrawal rates at longitudinal sections were also presented in Fig. 2(a<sub>2</sub>–f<sub>2</sub>), where more developed secondary dendritic arms were observed in Fig. 2(a<sub>2</sub>–e<sub>2</sub>), but only partial ones could be seen in Fig. 2(f<sub>2</sub>).

Based on the observations of the dendrite microstructures in Fig. 2, the schematic diagrams of the dendrite morphologies of single crystal

Download English Version:

<https://daneshyari.com/en/article/5450371>

Download Persian Version:

<https://daneshyari.com/article/5450371>

[Daneshyari.com](https://daneshyari.com)